Separation and Purification Technology 326 (2023) 124712

Contents lists available at ScienceDirect

Separation and Purification Technology

journal homepage: www.elsevier.com/locate/seppur

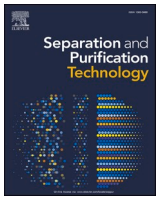

Membrane-assisted reactive crystallisation for the recovery of dissolved phosphorus in vivianite form from liquid effluents

R. Jiménez-Robles [a], V. Martínez-Soria [a], M. Izquierdo [a], Lo-I. Chen [b], K. Le Corre Pidou [b], E. J. McAdam [b,*]

[a] Research Group in Materials Technology and Sustainability (MATS), Department of Chemical Engineering, School of Engineering, University of Valencia, Avda. Universitat s/n, 46100 Burjassot, Spain
[b] School of Water, Energy and Environment, Cranfield University, Bedfordshire MK43 0AL, UK

ARTICLE INFO

Keywords:
Membrane-assisted crystallisation
Nanoparticles
Nucleation kinetic
Phosphorus recovery
Polymeric membrane
Vivianite

ABSTRACT

Novel membrane crystallisation processes resolve the mixing challenge on conventional crystallisers, by providing fixed interfacial area over which supersaturation is controlled for nucleation. Moreover, the membrane surface is thought to reduce interfacial energy and encourage micromixing. In this regard, a novel membraneassisted reactive crystallisation (MARC) process was used in this work for the dissolved phosphorous recovery in form of vivianite crystals from a phosphate-rich solution by means of the dosing of iron (II). To characterise the role of the boundary layer in controlling nucleation, a batch lab-scale system was used for the crystallization tests, and different hydraulic conditions (Reynolds ranging from 105 to 395) and polymeric membranes were tested. The crystallisation process was influenced by the hydraulic conditions, in which a low liquid velocity led to a lower induction time and vivianite supersaturation, and therefore, higher nucleation rates. Membrane properties were characterised to establish their role in the modification of the critical free energy requirement for nucleation, and for the promotion of micromixing, as possible factors that can be used to modify nucleation kinetics. As result, the bulk induction time tended to decrease with the increase in membrane hydrophobicity, roughness, pore size and porosity. Spherical vivianite nanoparticles were always synthesised with a mean size around 35 nm and a narrow distribution independently of the hydraulic conditions and membrane used. Finally, the crystallisation kinetic conformed to a diffusion-dependent nucleation mechanism, in which higher residence times for mixing increased the ion collision probability for nucleation. Importantly, this study demonstrated that MARC is an attractive prospect for nutrient recovery from wastewaters where crystal nucleation can be easily controlled by setting the operational conditions and membrane properties, eliciting considerable process intensification over existing conventional crystalliser.

1. Introduction

Phosphorus (P) is an essential element for life on Earth [1–3], being involved in the metabolic activity of plants and microorganisms among other biological and geological processes [2–6]. Consequently, P is also an important component of the most used fertilizers, whereas P compounds such as phosphoric acid and its derivates are valuable chemicals for the electronic industry and immobilization of heavy metals, among other applications [3,5,6,7]. However, the available P in nature, which is mainly obtained from the mining of phosphate rock (apatites) [2,7], is depleting at an accelerated rate due to the rising global demand, accordingly with population growth and improved living standards [2,8,9]. Thus, natural P sources are expected to be used up by the end of this century [2,6,7,10]. Therefore, the search and exploitation of new and renewable P sources are important to ensure the feasible supply of this element [6,11].

Urban wastewaters are a potential source of P which could be recovered in form of salts by means of crystallisation reactions [2]. The most common technique for P recovery in wastewater treatment plants is the crystallisation by the addition of Mg salts, leading to the formation of struvite ($(NH_4)MgPO_4{\cdot}6H_2O$) [11,12]. The large quantity of chemicals and the relative low efficiency of the process, coupled with the high capital cost of installation, hinder the application and feasibility at large-scale [1,2,10]. However, stricter environmental regulations are

* Corresponding author.
E-mail address: e.mcadam@cranfield.ac.uk (E.J. McAdam).

https://doi.org/10.1016/j.seppur.2023.124712
Received 13 June 2023; Received in revised form 31 July 2023; Accepted 1 August 2023
Available online 6 August 2023

lowering the admissible limit of P content in treatment plant effluents, and P recovery from wastewater has become a mandatory operation in some countries [2,9,13]. Therefore, an emergent need exists for the development of new processes that enable lower cost and higher efficiency P recovery.

Vivianite ($Fe_3(PO_4)_2{\cdot}8H_2O$) is a phosphate mineral that is naturally present in iron (Fe) and P rich environments under reducing conditions [14] such as in freshwater and marine sediments, and waterlogged and organic soils [2–5,14]. Different crystalline and amorphous phases are associated with vivianite-based compounds (vivianite, metavivianite, santabarbaraite…) [1–5]. Vivianite is considered a valuable chemical for its use as a slow-release fertilizer, for the production of lithium-ion batteries and in the electronic industry [2,6,14]. Vivianite presents an extremely low solubility in water [9,14], thereby, it could be easily obtained by precipitation of phosphates contained in a liquid matrix after the addition of a Fe^{2+} salt [1,15]. Frossard et al. [15] evidenced the presence of vivianite in wastewater sludge flocculated with $FeSO_4$. Compared with struvite, the synthesis of vivianite through precipitation could reduce operating costs of P recovery mainly due to an easier operation and lower consumption of chemicals [1,2,9]. The lower solubility limit of vivianite also implies that higher removal efficiencies can be achieved and may be viable for a broader range of feed water concentrations. Priambodo et al. [6] added a Fe^{2+} salt to a real wastewater from the electronic industry for the crystallisation of P in vivianite form in a fluidised bed crystalliser, reporting a P removal of 95 % at the optimal operational condition. Vivianite crystallisation can be influenced by several factors including Fe:P molar ratio, pH, temperature, microorganisms, organic matter, sulfate concentration, seed crystals, supersaturaion, and hydraulic conditions [1,2]. However, few studies on vivianite synthesis have been published [2,6,9], requiring greater depth in understanding of nucleation and crystal growth processes.

Supersaturation is the driving force for nucleation and crystal growth. Sparingly soluble salts such as vivianite require significant supersaturation to develop before induction. Mixing is also important as the increased likelihood for molecular collision can reduce the activation energy requirement for nucleation [16,17]. However, the regulation of supersaturation in existing crystallisers is extremely challenging due to the poorly defined hydrodynamic conditions, leading to inconsistent mixing of reactants [18–20]. This can result in overdosing of reactant and inconsistent crystal product quality which can be important for downstream applications. Membrane contactors offer fixed interfacial area to foster the homogeneous regulation of supersaturation, while the formation of a well-defined laminar boundary layer also creates a region of elevated supersaturation which is thought to enable the independent control of nucleation from crystal growth [19,21]. Consequently, membrane contactors offer greater control over nucleation, and their high interfacial area creates a more scalable and lower cost alternative to conventional equipment for separation and reactions processes [10,22–24]. In this context, membrane-assisted crystallisation (MAC) operation emerged as a promising technique for crystal production. MAC operation has primarily focused on evaporative crystallisation of high soluble aqueous salts, and antisolvent crystallisation for the production of high value but poorly soluble active pharmaceutical ingredients [20,25,26]. Likewise, membrane-assisted reactive crystallisation (MARC) operation is physically analogous to antisolvent crystallisation, as the membrane regulates the inclusion of liquid reactant into the reaction zone through an overpressure within the pores [18,22,27]. However, the mechanism of crystallisation is distinct since the reactant is used to raise supersaturation (MARC) rather than to reduce the solubility limit (evaporative and antisolvent crystallisation) [22]. While the concept has been proposed, MARC has been rarely studied. In principle, the membrane can provide a high level of micromixing [26,28–30], allowing high supersaturation indices and low induction times [31], since all the surface pores of the membrane could act as mixing points at a microscopic and molecular level [26,31,32]. The membrane has also been proposed to promote heterogeneous nucleation [19,22,33], by reducing the free energy barrier through advancing solute-membrane interactions [20,31]. Thus, the quality of the final crystals could be adjusted by the selection of the appropriate membrane properties and hydraulic conditions [22,34–36].

This study therefore examines how membrane crystallisation can be used to modify the nucleation kinetics for reactive sparingly soluble systems, to provide a controlled engineered environment for P recovery through vivianite crystallisation. The microporous membrane in MARC was used to facilitate dosing of an Fe^{2+} solution into a phosphate-rich solution, with the ambition to: (i) investigate how boundary layer conditions can be used to modify supersaturation leading to the advancement in regulation of nucleation kinetics by applying different hydrodynamic conditions inside the membrane module; (ii) study the effects of membrane properties to determine how they might regulate nucleation kinetics through their role in reducing critical surface free energy requirement for nucleation, and micromixing, and; (iii) develop a framework that can describe how nucleation kinetics can be modified by MARC by means of direct determination of induction time in the bulk solution and at the membrane. The direct determination of induction time is rarely reported, and is the basis for establishing new knowledge in vivianite crystallisation and for the development of membrane-assisted crystallisation as a platform technology for reactive systems.

2. Materials and methods

2.1. Experimental setup and vivianite crystallisation tests

The crystallisation tests for the P recovery in vivianite form by means of a MARC were conducted in the laboratory-scale system shown in Fig. 1. First, a phosphate stock solution at a concentration of 1.1 mM was prepared with sodium phosphate dibasic heptahydrate ($Na_2HPO_4{\cdot}7H_2O$, $\geq$ 99 %, Acros Organics, Geel, Belgium), and a ferrous stock solution (Fe^{2+}) at a concentration of 1.6 mM was prepared with iron (II) chloride tetrahydrate ($FeCl_2{\cdot}4H_2O$, $\geq$ 99 %, Sigma-Aldrich, Saint Louis, MI, USA). MilliQ water was used as the solvent for both solutions, and flushed with N_2 prior to use in order to remove the residual dissolved oxygen and avoid the oxidation of the ferrous ion [9,14]. Phosphate stock solution simulated a wastewater effluent rich in phosphates and prevented the potential interference of soluble or suspended compounds in the vivianite formation, which eased research purposes.

A 500 mL glass bottle was initially filled with 250 mL of the phosphate stock solution, and it was placed on a magnetic stirrer (Supernuova multi-place, Thermo Scientific, MA, USA) at 300 rpm with a 2 cm magnetic bar for the continuous agitation of the solution. Also, another 500 mL glass bottle was initially filled with 250 mL of the Fe^{2+} stock solution and placed on a precision balance (PCB, Kern & Sohn GmbH, Balinge, Germany) in order to carry out a mass balance. The headspace of both bottles was kept under a continuous N_2 flow to avoid the inclusion of oxygen into the solutions during the crystallisation tests.

A flat-sheet membrane was coupled inside a flat-sheet membrane module (FM) build in methacrylate with an effective contact area of 40 cm^2 (a picture of the FM can be found in supplementary material S1), and the permeate and retentate side of the FM were connected to the phosphate and Fe^{2+} solutions, respectively. Initially, the phosphate solution was recirculated through the permeate side at a liquid flow rate (Q_L) ranging from 8 to 30 L h^{-1} using a peristaltic pump (323, Watson-Marlow, Cornwall, UK), which resulted in liquid velocities between 2.8 and 10.4 cm s^{-1} what it meant Reynold numbers (*Re*) from 105 to 395 inside the FM. At these Q_L, the hydraulic residence time inside the permeate side of the module ranging from 1.0 to 3.6 s. The liquid velocity inside the FM was set based on a previous work [37]. Also, the Fe^{2+} solution was driven to the retentate side of the FM at a flow rate of 4.66 $\pm$ 0.12 mL min^{-1} with a peristaltic pump (Easy-Load Masterflex L/S, Cole Parmer, Illinois, USA), keeping the outlet port of the retentate side closed. The pressure increased in the retentate side of the FM as consequence of the continuous Fe^{2+} solution pumping, and the pressure

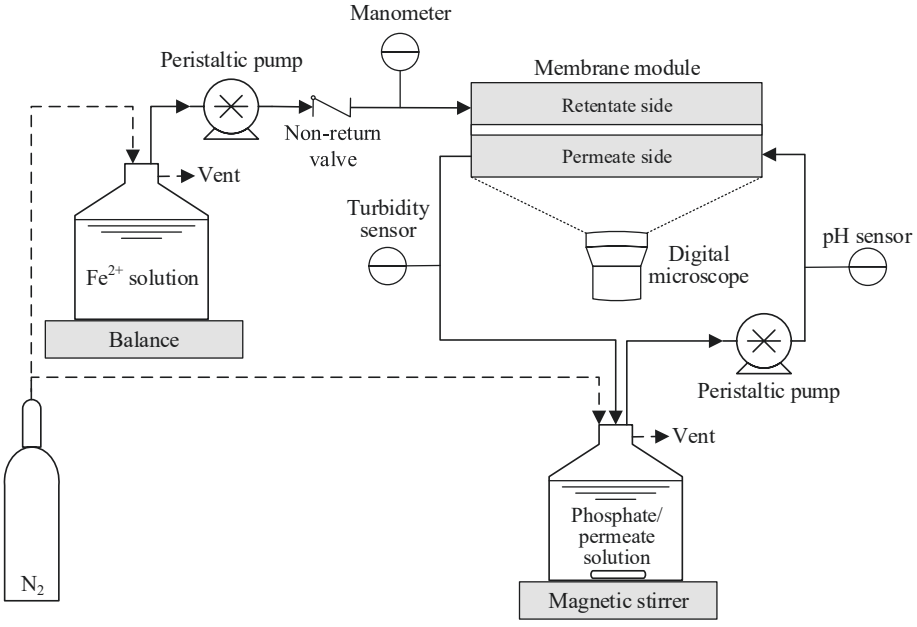

Fig. 1. Flowchart of the membrane-assisted reactive crystallisation for the phosphorus recovery in vivianite form. Continuous line denotes liquid stream, and dashed line denotes gas stream.

was monitored with a digital manometer (RS-8890G, RS Group, London, UK). The beginning of the crystallisation tests (t = 0) was set at the time in which the pressure of the retentate side reached the liquid entry pressure (LEP) of the membrane (Table 1), thereby, the dosing of Fe^{2+} into the permeate side started. The crystallisation test was stopped after the dosing of 250 mL of Fe^{2+} solution, resulting in an iron-to-phosphorus atomic ratio (Fe:P) of 1.5 in the phosphate/permeate solution. This Fe:P ratio satisfied the stoichiometry of the overall chemical reaction between Fe^{2+} and PO_4^{3-} for the vivianite formation (Eq. (1), and it has been reported as the optimal value for the vivianite formation [1]. Crystallisation tests were conducted at room temperature without additional control (21.3 ± 1.3 °C), since the temperature has a negligible effect on the solubility product of vivianite in this range of values [9,14].

$$3Fe^{2+} + 2PO_4^{3-} + 8H_2O \rightleftharpoons Fe_3(PO_4)_2 \cdot 8H_2O \quad (1)$$

Vivianite crystallisation was monitored based on the turbidity of the phosphate/permeate solution by means of a twin-axial turbidity probe (InPro 8200/Epoxy/120, Mettler Toledo, Leicester, UK) mounted at the outlet of the permeate side of the FM, which provides sensitive detection for the onset of nucleation. The turbidity profiles were used for the determination of bulk induction time and nucleation kinetics. In addition, the pH of the phosphate/permeate solution was monitored with a pH probe (Easy Ferm PlusPHI Arc 325, Hamilton Company, GR, Switzerland) and maintained at pH 7, at which vivianite formation is believed to dominate the Fe-P reactions [2,9]. The pH was adjusted [9] with the addition of 1 M sodium hydroxide (NaOH pellets, Fisher Chemicals, Loughborough, UK) and 1 M hydrochloric acid (HCl, 37 %, Fisher Scientific, Loughborough, UK) solutions. The total added volume of pH adjusting solutions during a test was always lower than 0.5 mL, thus this extra volume was neglected for further calculations. In order to analyse the scaling/deposition of solid particles onto the membrane, the membrane surface facing the permeate side was recorded throughout the crystallisation test using a digital microscope (Kopa, Ostec, Guangzhou, China). Frames were taken at different times of the tests from the recordings and processed with the ImageJ software (National Institutes of Health, USA) for the determination of membrane induction time and extent of the scaling/deposition [33]. Each crystallisation test was conducted in duplicate at the different experimental conditions tested in this work.

Immediately after the end of the test, a 5 mL sample of the phosphate/permeate solution was filtered in a vacuum filtration system using mixed cellulose esters filters with a pore size of 0.025 μm (MF-Millipore®, Merck KGaA, Darmstadt, Gerany) for the collection and ulterior analysis of the crystals. After the filtration, the filters were dried under a N_2 flow of 0.1 L min^{-1} overnight, and finally, they were stored in zip bags inside a desiccator.

The supersaturation index (SI) of the produced vivianite was estimated using the Visual MINTEQ 3.1 software (Swedish University of Agricultural Sciences, Sweden) based on the ratio of the ionic activity product (IAP) to the vivianite solubility product constant in water (K_{sp} = $1.82 \cdot 10^{-41}$ at 25 °C [9]) as SI = log (IAP / K_{sp}). Thus, SI was estimated in the bulk of the phosphate/permeate solution (SI_b) at the different PO_4^{3-} and Fe^{2+} concentrations with the test time, which were calculated from a mass balance conducted in the overall system (mass balance shown in supplementary material S2). Also, the SI inside the FM (SI_m) was estimated using mean PO_4^{3-} and Fe^{2+} concentrations values between the inlet and outlet of the permeate side based on a mass balance, relying on the time and Q_L (mass balance shown in supplementary material S3). This mass balance is intended only to illustrate the overall concentration gradient, since a complete description of mass transport within the boundary layer requires significant numerical analysis and validation to describe the relative role of local mixing.

Table 1
Main properties of the flat-sheet membranes used in this work: water contact angle (WCA), mean pore size (r_p), porosity (ε), root mean square roughness (R_q), and liquid entry pressure (LEP).

Membrane	WCA [b, °]	r_p [a], μm	ε [b], %	R_q [b], nm	LEP [b], bar
PVDF-St	36 ± 3	0.03	63 ± 2	163 ± 14	0.13 ± 0.04
Act_PVDF-Ds	87 ± 3	0.20	60 ± 5	573 ± 77	2.39 ± 0.58
PVDF-Ds	103 ± 2	0.20	62 ± 3	387 ± 63	2.79 ± 0.28
PVDF-Dp	119 ± 2	0.22	69 ± 1	548 ± 72	2.27 ± 0.02
Fun_PVDF-Ds	144 ± 2	0.20	59 ± 2	577 ± 89	2.98 ± 0.27
PTFE-1	148 ± 2	1.00	90 ± 5	202 ± 43	0.58 ± 0.13
PTFE-3	148 ± 2	3.00	91 ± 5	467 ± 91	0.57 ± 0.02
PP	154 ± 3	0.24	79 ± 5	269 ± 57	2.67 ± 0.10

[a] Provided by the manufacturer.
[b] Measured in this work.

2.2. Membrane materials and surface modification

A total of six microporous flat-sheet membranes were tested in this work: hydrophilic supported polyvinylidene fluoride (PVDF-St) (Trisep UB70, Microdyn-Nadir, Hessen, Germany), hydrophobic supported polyvinylidene fluoride (PVDF-Ds) (Dorsan Filtration S.L., Barcelona, Spain), hydrophobic unsupported polyvinylidene fluoride (PVDF-Dp) (Durapore, Merck KGaA, Darmstadt, Germany), two hydrophobic polytetrafluoroethylene with pore size of 1 and 3 μm (PTFE-1 and PTFE-3, respectively) (PF-1F and PF-3 W, respectively, Cobetter Filtration Equipment Co., Ltd., Hangzhou, China) and polypropylene (PP) (Accurel® PP-2EHF, 3 M Liqui-Cel, MN, USA). The main properties of the membranes are shown in Table 1. PVDF, PTFE, and PP represent common materials used in membrane modules for industrial applications and research purposes [19,31]. These membranes are considered as microfiltration (pore size > 0.1 μm) and ultrafiltration (pore size between 0.01 and 0.1 μm) membranes [38], so that, no retention of Fe^{2+} ions and water molecules were expected.

A modification technique of the PVDF-Ds membranes based on an initial alkali activation step followed by a functionalisation step was conducted in order to modify its hydrophobicity. This modification protocol was based on our previous works [39,40]. Thus, NaOH was used for the activation step, and 1H,1H,2H,2H-perfluorooctyltriethoxysilane (Dynasylan® F8261, Evonik GmbH, Essen, Germany) and 3-(triethoxysilyl)-propylamine (APTES, Sigma-Aldrich, Saint Louis, MI, USA) were used as the modifying agent and the silica precursor, respectively, for the functionalisation step. The activated and functionalised PVDF-Ds were denoted as Act_PVDF-Ds and Fun_PVDF-Ds, respectively, and their properties are shown in Table 1.

2.3. Analysis methods

The membrane surface hydrophobicity was evaluated by means of the measurement of the static water contact angle (WCA, °) with a goniometer (OCA25, DataPhysics, Filderstadt, Germany), following the sessile drop technique [41] in which a water droplet of 5 μL was placed onto the membrane surface at room temperature. An image of the water droplet was taken at 3 s and the WCA was determined with the SCA20 software (DataPhysics, Filderstadt, Germany). The WCA was evaluated at different surface locations on the membrane and a mean value was obtained from at least five measurements, using the standard deviation as a measure of the associated error.

The overall porosity (ε, %) of the membranes was gravimetrically measured with 1-octanol (99 %, Acros Organics, Geel, Belgium), and the procedure can be found elsewhere [42,43]. Briefly, 2x2 cm samples were weighed and immersed in vials with 10 mL of 1-octanol. The vials were kept in an orbital shaker for 2 h at room temperature. Finally, the membranes samples were surface dried with absorbent paper and weighed. At least five samples of each membrane were analysed.

The liquid entry pressure (LEP, bar) of the membranes was evaluated using the same experimental setup detailed previously for the crystallisation tests. A membrane sample was placed inside the FM, the outlet port of the retentate side was kept closed, and the ports of the permeate side were opened to the atmosphere. Deionised water was pumped inside the retentate side at a flow rate of ~ 5 mL min^{-1} in order to increase the pressure slowly and gradually, and the membrane surface of the permeate side was continuously monitored with the digital microscope. The pressure at which the first drop appeared on the membrane surface was established as the LEP. At least five measurements were conducted for each membrane.

Membrane roughness was determined by atomic force microscopy (AFM) in tapping mode (Digital Instruments, Dimension 3100 SPM with Nanoscope V controller, Veeco Instruments, Inc., NY, USA), using AFM probes with a force constant and length of 42 N/m and 125 μm, respectively (PPP-NCHR, Nanosensors™, Neuchatel, Switzerland). Images of the membrane topography were taken with a size scan of 25x25 μm, and Gwyddion data analysis software (Department of Nanometrology, Czech Metrology Institute, Brno, Czech Republic) was used for image processing and determination of the root mean square roughness (R_q, nm). A mean value of R_q was determined in at least three different locations of the surface.

Crystal size and shape was analysed by field emission scanning electron microscopy (FESEM) at an accelerating voltage of 10 kV (Tescan Vega 4, Tescan Orsay Holding, a.s., Kohoutovice, Czech Republic). The microscope was equipped with an energy dispersive x-ray (EDX) spectrometer, which was used for the atomic content determination of different elements. For image acquisition, the filter samples with the collected crystals were previously placed on a metal holder and then coated with a fine layer of Au. The mean crystal size was obtained by measuring the diameter of at least 300 particles from three FESEM images with the abovementioned ImageJ software.

X-ray diffraction (XRD) analysis was carried out for the identification of crystalline phases in the solid particles formed in the crystallisation tests. The diffractograms were obtained with an XRD system (AXS D8 ADVANCE A25, Bruker, MA, USA) and the patterns were processed with QualX2.0 software (Software IC, Institute of Crystallography – CNR, Bari, Italy).

2.4. Crystallisation kinetic analysis

Nucleation kinetics were characterised for vivianite, assuming that only primary nucleation was of relevance due to the low solubility of vivianite [44]. The nucleation rate of vivianite expressed in mass basis (r, mg L^{-1} min^{-1}) was assumed to be the supersaturation rate at the bulk induction time [45]:

$$r = \frac{C_{viv}^{ind}}{t^{ind}} M_{viv} \quad (2)$$

where C_{viv}^{ind} (M) is the mean concentration of vivianite inside the FM at bulk induction time (t^{ind}, min), and M_{viv} is the molar mass of vivianite (501610 mg mol^{-1}). For the estimation of C_{viv}^{ind}, a complete reaction between Fe^{2+} and PO_4^{3-} towards vivianite, and no secondary reactions were assumed (mass balance shown in supplementary material S3).

The empirical power-law relationship between the nucleation rate and supersaturation (S) developed by Sangwal (2009) [46] was used to determine whether the primary nucleation kinetic inside the FM was in accordance with the classical nucleation theory (CNT) principles [46]:

$$r = k\left(\ln S_m^{ind}\right)^m \quad (3)$$

where *m* is the so-called the apparent nucleation order, *k* is the nucleation constant related with the number of stable nuclei forming per unit volume per unit time, and S_m^{ind} is the supersaturation of the vivianite inside the FM at bulk induction time calculated as follows:

$$S_m^{ind} = \frac{C_{viv}^{ind}}{C_{viv}^{*}} \quad (4)$$

where C^*_{viv} is the solubility of the vivianite calculated from the K_{sp} ($C^*_{viv} = 3.47 \cdot 10^{-9}$ M from a $K_{sp} = 1.82 \cdot 10^{-41}$ at 25 °C [9]). The linearization of Sangwal's power-law yields:

$$\ln(r) = \ln(k) + m \cdot \ln\left(\ln\left(S_m^{ind}\right)\right) \quad (5)$$

3. Results and discussion

3.1. Effect of hydrodynamic conditions in the vivianite crystallisation

Crystallisation tests were conducted with the PVDF-St membrane at different *Re* to evaluate the role of the boundary layer in modifying the nucleation rate of vivianite. The turbidity of the phosphate/permeate solution always kept in 0 until the bulk induction time was reached, and then the turbidity started to increase with the operation time (Fig. 2a),

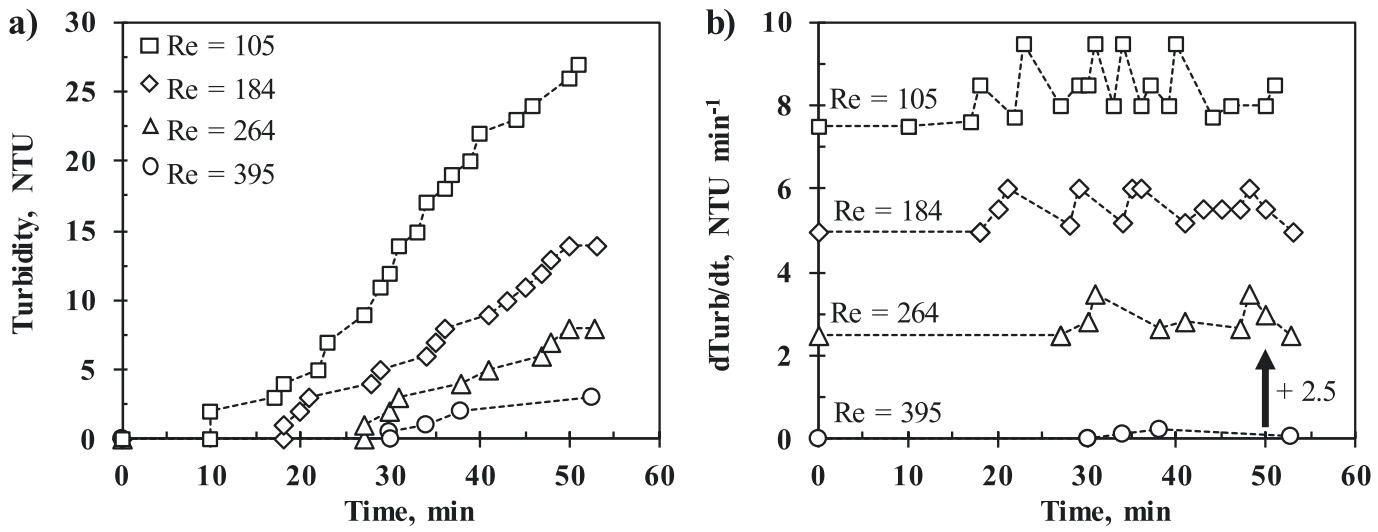

Fig. 2. a) Representative turbidity profiles and b) their derivatives of the turbidity with respect to the time (dTurb/dt) of the phosphate/permeate solution with the time of the crystallisation test with PVDF-St membrane at different Reynold numbers inside the membrane module (Re).

indicating a continuous crystallisation in the bulk of the phosphate/permeate solution. According to the simulations carried out with Visual MINTEQ for the system used in this work, the Fe and P were initially in the form of Fe^{2+}, HPO_4^{2-} and $H_2PO_4^-$. Moreover, the speciation of the Fe and P were in accordance with those reported by other authors [9,14]. Thus, the chemical reactions involved in the current system for a pH of 7 were presumed to lead mainly to the formation of vivianite from Fe^{2+} with protonated phosphate (Eq. (6) and (7) [9,14] instead of free phosphate (Eq. (1).

$$3Fe^{2+} + 2HPO_4^{2-} + 8H_2O \rightleftharpoons Fe_3(PO_4)_2 \cdot 8H_2O + 2H^+ \quad (6)$$

$$3Fe^{2+} + 2H_2PO_4^- + 8H_2O \rightleftharpoons Fe_3(PO_4)_2 \cdot 8H_2O + 4H^+ \quad (7)$$

Turbidity evidenced the onset of nucleation (bulk induction time). The time at which turbidity commenced was delayed when *Re* was increased from 105 to 395 (Fig. 2a). Following nucleation, the turbidity continued to increase, reaching a maximum value of 27 ± 4 NTU at *Re* 105. In comparison, a lower final turbidity of 4 ± 1 NTU was obtained in the test conducted at the highest *Re* of 395. This indicates that nucleation rate could be increased through modifying process hydrodynamics. We suggest this is due to the reduction in Fe^{2+} reactant concentration within the boundary layer as the liquid velocity increased which involved a lower residence time in the reaction zone near the membrane (permeate side).

The turbidity profiles presented a stepped tendency from the bulk induction time until the end of the crystallisation test (Fig. 2a). In order to elucidate this tendency, a differential analysis of the turbidity profiles was conducted, in which the derivative of the turbidity with respect to time (dTurb/dt) were calculated by regressive differences, and this derivative represented the nucleation rate (Fig. 2b). The obtained dTurb/dt curves evidenced the stepped tendency of the profiles, showing a periodical increase in the nucleation rate in form of peaks followed by a decline. These peaks may indicate exceedance of the primary nucleation threshold, where sufficient supersaturation has been achieved to overcome the energy barrier to create formation of a new crystal phase. The frequency and height of the peaks were greater as *Re* decreased, indicating higher overall nucleation rates and a greater frequency of new nucleation events.

At the outset of dosing, the SI increased rapidly due to the injection of new reactant (Fig. 3). Within this initial phase, the estimated SI of vivianite was slightly higher in the membrane module compared to the bulk solution, but became comparable following the progressive addition of injection volume which gradually diluted P in the system (Fig. 3a). A similar observation was made when modifying *Re*, where the concentration within the membrane was slightly elevated at the lowest *Re* but tends toward an equivalent value independent of *Re* following the continued addition of reactant (Fig. 3b). The negligible influence of *Re* in estimated SI may be attributed to the low solubility of vivianite, since

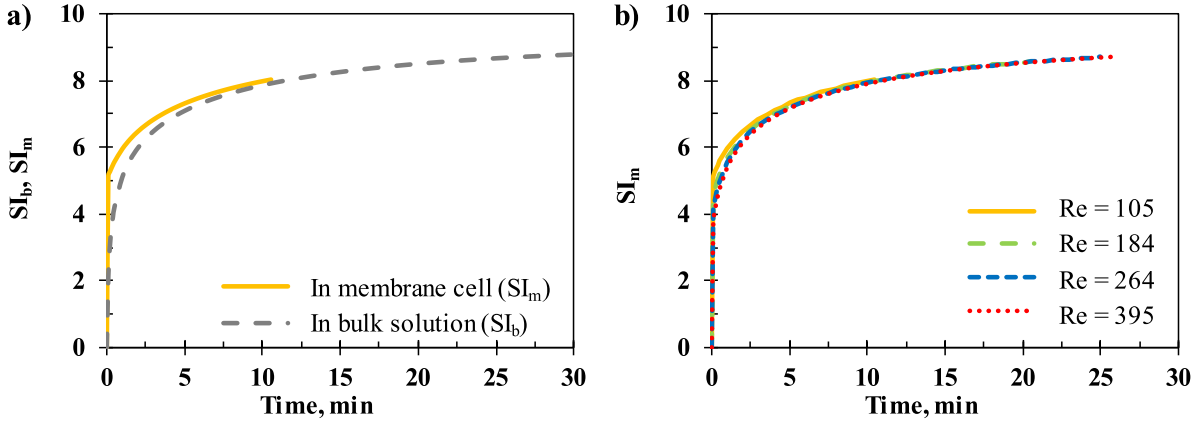

Fig. 3. a) Supersaturation index (SI) estimated inside the bulk phosphate/permeate solution (SI_b) and inside the membrane module (SI_m) with the time of crystallisation test at a Reynold (Re) of 105. b) SI_m with the time of crystallisation test at different Re. SI_m was estimated until the bulk induction time at each Re.

sparingly soluble substances reach high supersaturation levels very quickly [44]. However, two aspects should be considered: (i) the SI values were estimated based on mean concentration mass balances, and so do not take into consideration the relative ratio of the shear component to the diffusivity for mass transfer occurring within the boundary layer, which will be modified by *Re* and could lead to relatively higher local supersaturation, which would increase the nucleation rate [20]; and (ii) the high level of micromixing provided by the porous membrane [31,34] may enhance the mass transfer of the reactants at molecular level and add turbulence in the boundary layer [27]. These phenomena could increase the collision frequency of the reactive ions, lowering the activation energy for nucleation [16,17]. Thus, longer residence times at low *Re* would increase the probability for mixing and ion collision inside the membrane module, accelerating the nucleation especially for sparingly soluble salts due to their low ion densities. The higher local supersaturation and ion collision probability at lower *Re* was in agreement with the experimental results (Fig. 2). Thus, the integration of the membrane technology in a crystallisation process was demonstrated to allow the control of the nucleation by setting the hydrodynamic conditions.

The induction time is defined as the time difference between the solution achieving a saturated state (SI = 0, or C/C* = 1) and the time in which the solid particles were detected for first time in the phosphate/permeate solution (bulk induction time) and in the membrane surface (scaling induction time). The induction time therefore represents the time in which the crystallising system is in a metastable state, and according to CNT is inversely proportional to the nucleation rate [45–47]. The bulk induction time increased markedly from 10.5 ± 0.7 min ($SI_m \approx 7.9$) to 22.7 ± 4.0 min ($SI_m \approx 8.6$) at a *Re* of 105 and 184, respectively, for the crystallisation tests carried out with the PVDF-St membrane (Fig. 4), whereas an apparent plateau was achieved in induction for Re $\geq$ 184 with values of around 25 min ($SI_m \approx 8.7$). Shorter induction times corresponded to higher turbidity increase within the phosphate/permeate solution (Fig. 2a). Therefore, higher nucleation rates were inferred for lower SI which does not generally conform with CNT. Hence, these results suggested that the local supersaturation, mixing effect and/or the increased probability of ion collision within the boundary layer could be especially favoured at the lowest *Re*, raising the nucleation rate.

To elucidate the potential mechanisms for vivianite crystallisation, scaling induction time was also determined for the crystallisation tests using PVDF-St membrane at different *Re* (Fig. 4). An example of image processing for scaling analysis can be found in supplementary material S4. The scaling induction time was always in mean values around 12 min, independently of the *Re*, which may indicate that scaling was more closely controlled by dose rate, dose concentration and/or membrane properties, as these were fixed for each condition. At low Re, bulk nucleation seemingly occurred before scaling suggesting that scaling is likely to be dominated by deposition rather than through an adhesive growth mechanism and can therefore be controlled through hydrodynamics and system orientation (i.e. vertical alignment to avoid sedimentation). However, for higher *Re* where lower nucleation rates were observed, scaling was observed before bulk nucleation. While this may also be due to the deposition of crystals formed within the reaction zone near the membrane surface, the role of the membrane properties in promoting heterogeneous nucleation cannot be discounted.

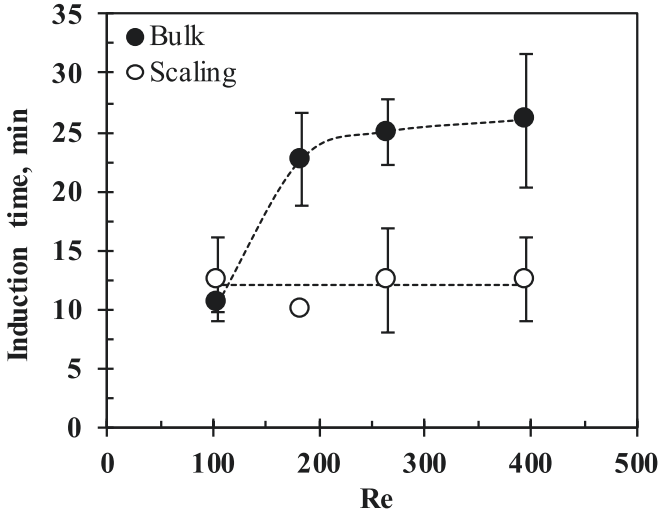

Fig. 4. Bulk and scaling induction time versus Reynold number (Re) in the permeate side of the membrane module for crystallisation tests with PVDF-St. Error bars denotes the standard deviations.

3.2. Effect of the membrane material and properties

Membrane materials of different properties were evaluated to determine their role in lowering the free energy requirement of nucleation, and/or their role in modifying local mixing conditions to shorten induction time. In this work, the supersaturation rate was fixed in the crystallisation tests, unlike previous research that have looked at these properties such as in membrane distillation or osmotic crystallisation, in which the flux (and hence supersaturation rate) was modified as a function of the membrane properties, making it difficult to provide an independent assessment of the relative role of material properties. In order to elucidate the individual effect of each membrane property, *Re* was fixed to 105, and the induction time was plotted against the WCA, R_q, r_p and ε (Fig. 5). The bulk induction time was in values of around 12 min for a WCA ranging from 36° to 103°, and then the induction time suddenly declined to values around 6 min for a WCA from 119° to 154° (Fig. 5a). This result suggested that the WCA range from 103° to 119° marked a transition zone in which the kinetic and thermodynamic behaviour of the vivianite nucleation changed, leading to higher nucleation rates when membranes with a WCA higher than 119° were used. A similar behaviour was observed with the membrane porosity, in which values between 60 and 65 % led to induction times $\gtrapprox$ 10 min, whilst higher ε values (>65 %) lowered the induction times to values of around 6 min (Fig. 5b).

In general terms, the bulk induction time tended to decrease with membrane roughness and pore size (Fig. 5c and d), leading to higher nucleation rates. However, the PVDF-Ds and Act_PVDF-Ds membranes with a R_q of 387 and 573 nm, respectively, were out of the tendency, showing an induction time of ~ 12 min (Fig. 5c) likely due to the lower WCA ($\leq$103°). Regarding the pore size, this tendency was not observed in membranes with a r_p of ~ 0.2 μm which led to induction times between 4.5 and 12.5 min (Fig. 5d), likely due to the conflation of different properties. These results suggest that membrane roughness and pore size present a smaller effect on encouraging nucleation than other properties such as WCA and porosity. While this analysis indicates that nucleation kinetics can be modified using membrane properties, this may have occurred due to synergistic effects. For example, although micromixing may be enhanced by single properties such as porosity, multiple converging factors (e.g. WCA, R_q and r_p) will likely define local fluid velocities and mixing patterns, that can serve to lower the activation energy requirement for nucleation.

The influence of membrane properties in conditioning induction time can also be ascribed to the critical surface free energy requirement for nucleation. The presence of a solid substrate (membrane) decreases the interfacial free energy, which also leads to a reduction of the nucleation energy barrier [48]. Therefore, the membrane surface can promote heterogeneous nucleation, allowing the crystallisation onset at lower supersaturation ratios than in the homogeneous case [19,22]. However, there is a lack of models in the literature which consider the different membrane properties in modifying the nucleation energy barrier. While instructive for membrane design, the most common model which relates membrane hydrophobicity and porosity to the

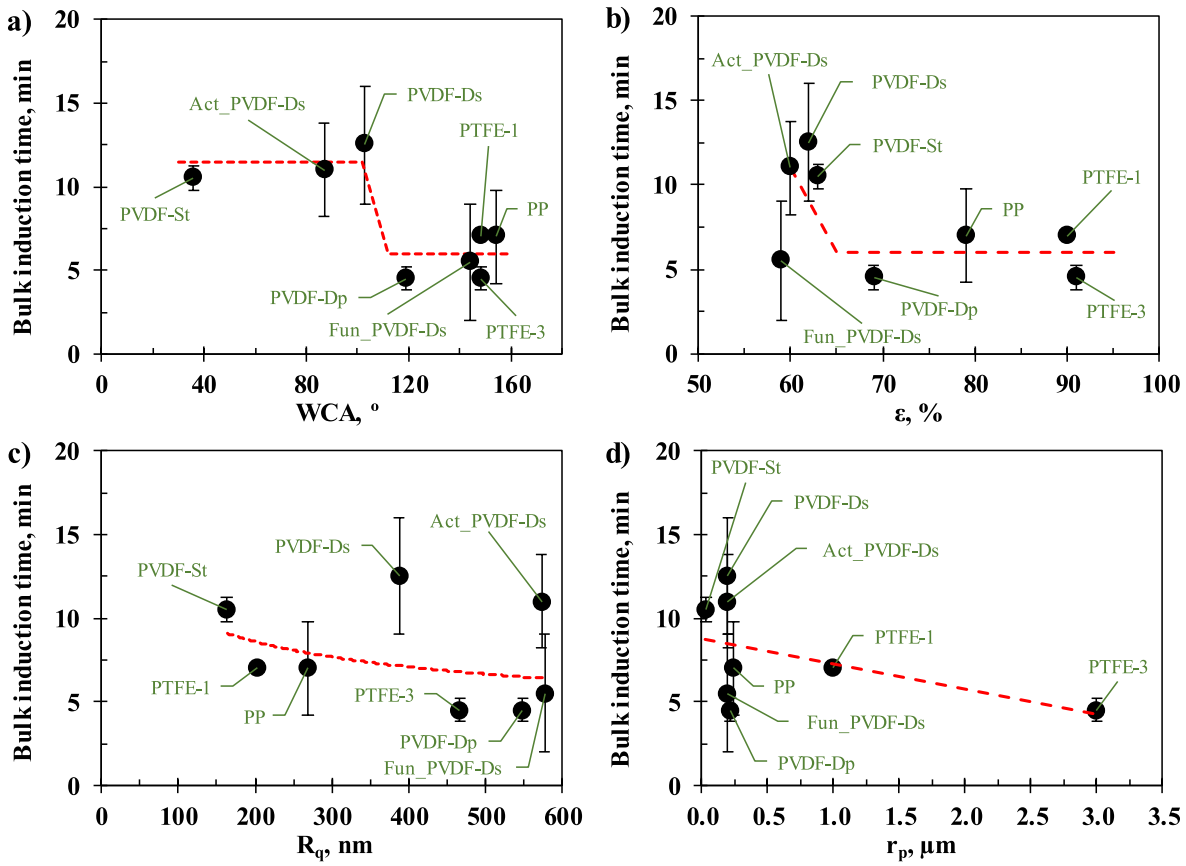

Fig. 5. Bulk induction time in the crystallisation tests versus membrane a) water contact angle (WCA), b) porosity (ε), c) root mean square roughness (R_q), and d) pore size (r_p), at a Reynold of 105. Membrane nomenclature as in Table 1.

preferential heterogeneous nucleation [21,49–51] cannot provide a unified perspective on the probability for heterogeneous nucleation on porous surfaces (model shown and discussed in supplementary material S5). This may be due to competing factors in material design, that can similarly modify Gibbs free energy requirement for nucleation through competing mechanisms (e.g. solute entrapment) [19]. There is also recognition that despite the high interfacial energy requirement of sparingly soluble salts setting a high surface free energy requirement for nucleation, the supersaturation (volumetric free energy) requirement to create the critical nucleus is sufficiently high for primary nucleation to proceed via a homogeneous mechanism that is therefore less dependent on membrane properties [44].

3.3. Crystallisation kinetic inside the membrane module

The power-law model proposed by Sangwal [46] was used to relate how membrane parameters and flow conditions inform nucleation kinetics based on CNT, where the supersaturation rate is an analogy to the primary nucleation rate (r) at induction. Higher primary nucleation rates were identified at shorter induction times, in which r increased from 3.40 to 5.69 mg L^{-1} min^{-1} as the bulk induction time decreased from 26.0 to 4.0 min (Fig. 6a). This is in accordance with CNT, where the

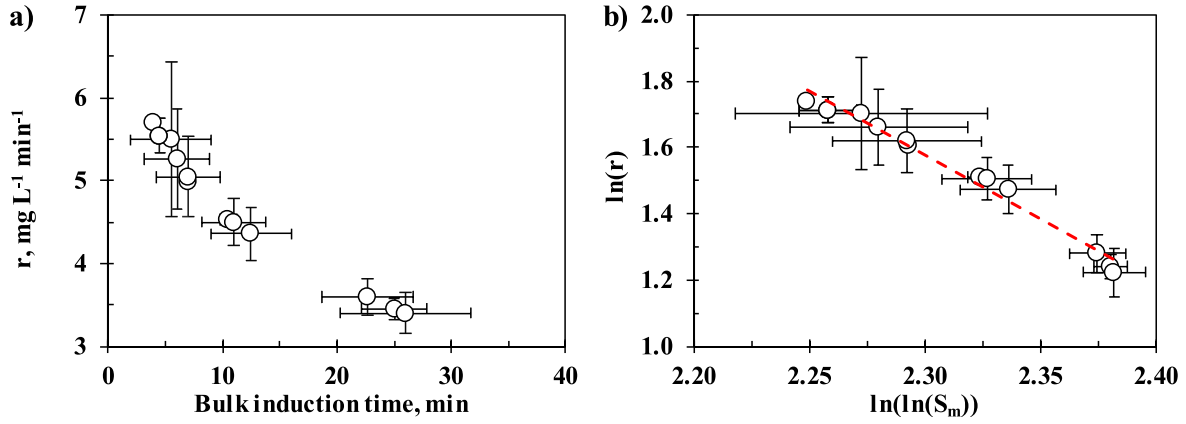

Fig. 6. a) Nucleation rate (r) versus bulk induction time, and b) Sangwal's power law relationship between nucleation rate and supersaturation level inside the membrane module (S_m) at the bulk induction time. All the crystallisation tests under the different operational conditions and membranes has been included in the graphs.

longer induction times corresponded with the lower turbidity data that was experimentally observed (Fig. 2a). In conventional crystallisers and according to CNT, higher nucleation rates are ordinarily facilitated within a region of elevated supersaturation (wider metastable zone width). However, in this study, higher nucleation rates were associated to a lower vivianite supersaturation at induction (Fig. 6b). This can be explained by an ion-dependent collision mechanism [16,17] in which the higher supersaturation rates promote greater mixing and a higher ion collision probability to reduce the activation energy requirement for nucleation. This effect could be facilitated by a low residence time and a high membrane hydrophobicity and porosity, resulting in higher nucleation rates, as experimentally observed. Thus, non-classical nucleation mechanisms, nanoscale phenomena, and macroscale dynamics should be considered for the evaluation of precipitation kinetic of vivianite through a MARC process in future studies.

A linear tendency was observed (R^2, 0.98) between the supersaturation achieved and supersaturation rate that was set either by a modification of *Re* (105–395) or discrete changes to membrane properties at a fixed *Re* 105 (Eq. (5) (Fig. 6b). The kinetic parameters of the model *m* and *k* showed values of −3.848 and 33691 mg L^{-1} min^{-1}, respectively, for this system. The low value of the apparent nucleation order *m* indicates a low energy barrier for formation of stable nuclei [46] which could result from the high micromixing in the boundary layer, complemented by the *relatively* high supersaturation achieved for vivianite induction. Therefore, nucleation kinetics conform more closely to a diffusion-dependent rather than a supersaturation-dependent nucleation mechanism, which has been previously recognised for sparingly soluble reactive salts [16,17]. The correlated kinetic response of nucleation to system modifications by membrane properties and hydrodynamics emphasise the extent to which the reaction zone within MARC may offer control over nucleation, and could be further regulated through adjustments in dosing rate and dose concentration to broaden the range of supersaturation trajectories that could be delivered.

3.4. Characterisation of the vivianite particles

The solid particles formed during the crystallisation tests were collected from the phosphate/permeate solution and analysed by microscopy and spectroscopy to determine their morphology, particle size and composition. Nanoparticles were always observed with a spherical and a smooth shape and no conglomerates were observed in any of the crystallisation tests (Fig. 7). The presence of nanoparticles and their glassy-like form (showing no faces) is ascribed to very fast nucleation rates within regions of high *relative* supersaturation [52]. This could indicate that the reaction zone for nucleation was located in the boundary layer, where a high local supersaturation was inferred (SI > 11). In contrast, a lower vivianite SI between 4 and 11 has been reported for conventional crystallisers, leading to lower nucleation rates and, consequently, the crystal growth was favoured resulting in bigger crystal sizes (>1000 nm) [9]. In this work, the particle size distribution was very narrow with mean particle sizes ranging from 29 to 44 nm and standard deviations lower than 10 nm (Table 2). Hence, the vivianite crystallisation mechanism in the bulk solution was independent of the membrane properties and hydraulic conditions tested. In sparingly soluble systems, high nucleation rates quickly consume the available ions within solution, resulting in a high number of small crystals, and since the ions are diffuse and the supersaturation is consumed by the production of new nuclei, crystal growth is limited. The consistency in particle size may be due to the confined length of the reaction zone in the membrane where the supersaturation is consumed particularly quickly, and the Fe^{2+} dosing was consistently applied. Increasing Fe^{2+} dose would assure non-limiting reaction conditions within the boundary layer, while a longer reaction zone (longer membrane) can supply a greater degree of supersaturation with an extended residence time to encourage growth of newly formed nuclei. Importantly, this study also demonstrates how membrane crystallisation can be applied for the consistent formation of nanocrystals with a tight crystal size distribution which is important for a range of critical applications, such as the production of long acting injectable medicines, through stricter control over nucleation [19,31,36]. The synthesis of vivianite in form of

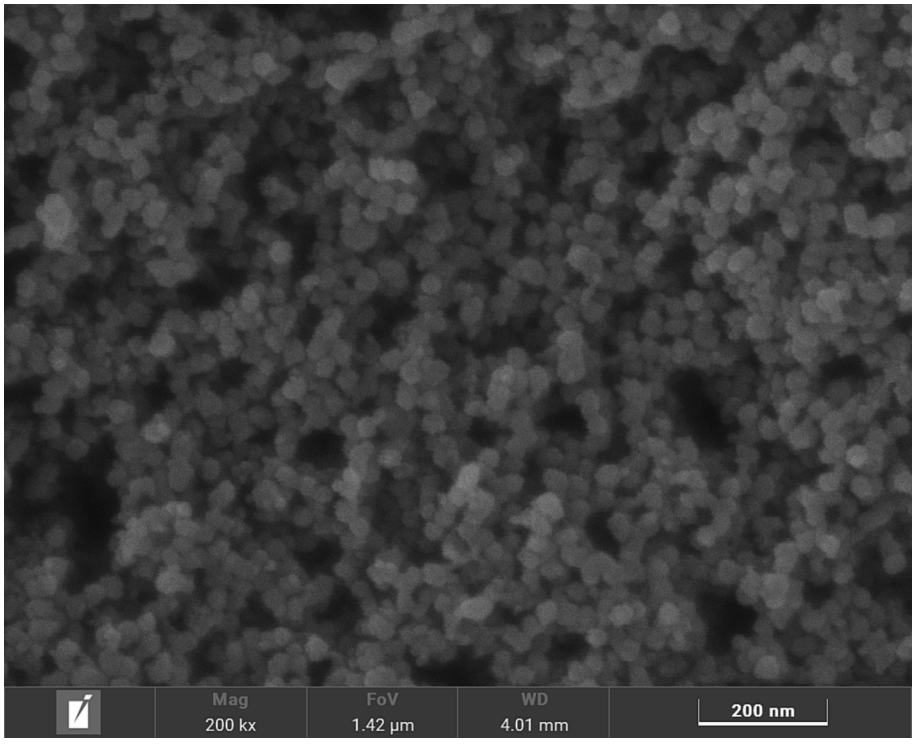

Fig. 7. FESEM images of the solid particles collected from the phosphate/permeate solution at the end of the crystallisation tests at a Reynold of 105.

Table 2
Mean particle size of the solid particles collected at the end of the crystallisation tests with different membranes and at different Reynolds (Re). The error denotes the standard deviation of the mean particle size distribution.

With different membranes at Re = 105	
Membrane	**Mean particle size, nm**
PVDF-St	43 ± 9
Act_PVDF-Ds	34 ± 8
PVDF-Ds	35 ± 8
PVDF-Dp	30 ± 7
Fun_PVDF-Ds	36 ± 10
PTFE-1 μm	29 ± 8
PTFE-3 μm	29 ± 8
PP-2E	29 ± 7
With PVDF-St at different Re	
Re	**Mean particle size, nm**
105	43 ± 9
184	39 ± 9
264	44 ± 10
395	31 ± 7

nanoparticles could favour a high purity product and ease its further separation from the liquid matrix. This product represents an interesting slow-release fertiliser with a high market price (10000 € t^{-1}, [1]). Hence, vivianite recovery by a MARC process seems an attractive alternative to fossil-based fertilisers or even struvite recovered by precipitation with a lower market price (500 € t^{-1}, [2]).

The composition of the collected particles was analysed by EDX, and Fe:P atomic ratio values ranging from 1.9 to 3.3 were obtained, with no appreciable tendencies between the different operational conditions. The Fe:P atomic ratio for pure vivianite is 1.5, which was the set condition for performing the crystallisation tests. The obtained higher ratios indicated a higher presence of Fe compounds different from vivianite, likely attributed to OH^- -bound in form of iron hydroxides [1,2,9,14]. The XRD pattern of the collected particles did not show crystalline peaks (Fig. 8), which suggested the presence of oxidised and poorly crystalline forms of vivianite, such as santabarbaraite ($Fe_3^{3+}(PO_4)_2(OH)_3{\cdot}5H_2O$), lipscombite ($Fe^{2+}Fe_2^{3+}(PO_4)_2(OH)_2$), and strengite ($FePO_4{\cdot}2H_2O$) [5,53]. Thus, these outcomes suggested a precipitation mechanism instead of a crystallisation pathway. Further analysis using different methodologies are required to better characterise the crystallinity of this type of particle in depth. While further work is required, we suggest the crystallinity may be modified through local adjustments of reactants and reaction rate. The colour of the collected particles in this work was of yellowish-brown hue (supplementary material S6) which could be related to the presence of iron hydroxides and santabarbaraite [6,53]. For the conditions examined, we therefore suggest that the MARC led to formation of amorphous vivianite-based particles and iron hydroxides. While the effective removal of phosphorus through this crystallisation pathway is compelling, further research on vivianite recovery is warranted to avoid the consumption of Fe^{2+} reactant in secondary reactions, particularly if it is the purity and crystallinity of the recovered vivianite that is critical to its downstream application.

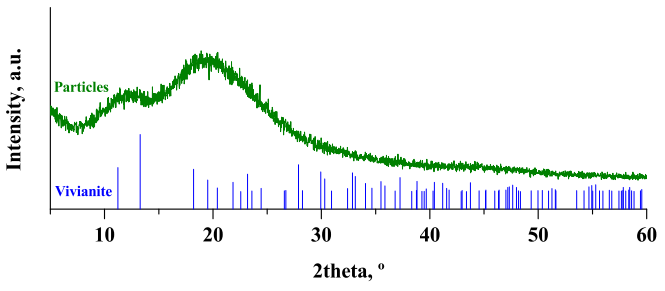

Fig. 8. XRD diffractogram of the collected solid particles from the crystallisation tests and reference peaks of pure vivianite from [4]. Intensity expressed in arbitrary units (a.u.).

4. Conclusions

The membrane-assisted reactive crystallisation has been demonstrated as a useful approach for controlling and modifying nucleation processes, unlike conventional stirred tank crystallisers where the poor mixing levels lead to overdosing of reactant and heterogeneous crystal product quality. Thus, a membrane crystallisation process has been introduced to enable the vivianite crystallisation for phosphorus recovery from a liquid effluent by the dosing of an iron (II) solution. The nucleation process was continuously monitored based on the turbidity of the solution which allowed the direct determination of induction time as well as provided useful information regarding nucleation rate. Lower induction times were obtained at lower liquid velocities, leading to higher nucleation rates. Thus, crystal nucleation was strongly influenced by the boundary layer in the interphase membrane-liquid, therefore, the nucleation could be controlled by the hydrodynamic conditions inside the membrane module. In addition, the integration of a porous membrane in the vivianite crystallisation process facilitated the micromixing of the reactants and lowered the energy barrier for nucleation. Therefore, the nucleation could also be controlled by selecting the appropriate membrane properties, in which the induction time tended to decrease as the membrane hydrophobicity, roughness, pore size, and porosity increased.

Finally, the nucleation kinetic was modelled using the Sangwal's power law based on the classical nucleation theory. This kinetic analysis showed that higher nucleation rates were associated to a lower vivianite supersaturation which may indicate an ion-dependent collision mechanism (non-classical nucleation). Thus, the membrane-assisted reactive crystallisation operation seemed to promote greater mixing and a higher ion collision probability which could reduce the activation energy requirement for nucleation even at low supersaturation degrees. Hence, the nucleation rate was related to the boundary layer and mixing conditions, which allows a strict control of the nucleation as a function of the operational condition set.

This work represents the first integration of membrane technology in phosphorus recovery from water in form of vivianite which has been demonstrated to be a practical approach for controlling vivianite crystallisation. Thus, a membrane-assisted reactive crystallisation can ease the prospect of phosphorus recovery in vivianite to realise benefits to cost and yield at large-scale processes, while also taking advantage of downstream value due to a homogeneous quality of crystals.

Funding

This research was funded by European Research Council Starting Grant "*Sustainable Chemical Alternatives for Reuse in the Circular Economy* (SCARCE, ERC StG #714080). PhD grant of R. Jiménez-Robles was funded by Ministerio de Universidades, Spain (Beca de Formación de Profesorado Universitario FPU19/02478). The research stay of R. Jiménez-Robles at Cranfield University was funded by Ministerio de Educación y Formación Profesional, Spain (Ayudas Complementarias para Estancias Breves y Traslados Temporales EST22/00167).

CRediT authorship contribution statement

R. Jiménez-Robles: Conceptualization, Data curation, Formal analysis, Investigation, Methodology, Writing – original draft. **V. Martínez-Soria:** Conceptualization, Funding acquisition, Methodology, Project administration, Supervision, Writing – review & editing. **M. Izquierdo:** Conceptualization, Data curation, Formal analysis, Funding acquisition, Investigation, Methodology, Project administration, Supervision, Writing – review & editing. **Lo-I. Chen:** Conceptualization, Data curation, Formal analysis, Investigation, Methodology. **K. Le Corre**

Pidou: Methodology, Project administration, Supervision, Writing – review & editing. **E.J. McAdam:** Conceptualization, Funding acquisition, Methodology, Project administration, Supervision, Writing – review & editing.

Declaration of Competing Interest

The authors declare that they have no known competing financial interests or personal relationships that could have appeared to influence the work reported in this paper.

Data availability

Data underlying this paper can be accessed through the following DOI: 10.17862/cranfield.rd.23977134.

Acknowledgements

None

Appendix A. Supplementary material

Supplementary data to this article can be found online at https://doi.org/10.1016/j.seppur.2023.124712.

References

[1] J. Zhang, Z. Chen, Y. Liu, W. Wei, B.J. Ni, Phosphorus recovery from wastewater and sewage sludge as vivianite, J. Clean. Prod. 370 (2022), 133439, https://doi.org/10.1016/j.jclepro.2022.133439.
[2] Y. Wu, J. Luo, Q. Zhang, M. Aleem, F. Fang, Z. Xue, J. Cao, Potentials and challenges of phosphorus recovery as vivianite from wastewater: A review, Chemosphere. 226 (2019) 246–258, https://doi.org/10.1016/j.chemosphere.2019.03.138.
[3] M. Nanzyo, H. Onodera, E. Hasegawa, K. Ito, H. Kanno, Formation and Dissolution of Vivianite in Paddy Field Soil, Soil Sci. Soc. Am. J. 77 (2013) 1452–1459, https://doi.org/10.2136/sssaj2012.0437n.
[4] M. Rothe, T. Frederichs, M. Eder, A. Kleeberg, M. Hupfer, Evidence for vivianite formation and its contribution to long-term phosphorus retention in a recent lake sediment: A novel analytical approach, Biogeosciences. 11 (2014) 5169–5180, https://doi.org/10.5194/bg-11-5169-2014.
[5] M. Rothe, A. Kleeberg, M. Hupfer, The occurrence, identification and environmental relevance of vivianite in waterlogged soils and aquatic sediments, Earth-Science Rev. 158 (2016) 51–64, https://doi.org/10.1016/j.earscirev.2016.04.008.
[6] R. Priambodo, Y.J. Shih, Y.H. Huang, Phosphorus recovery as ferrous phosphate (vivianite) from wastewater produced in manufacture of thin film transistor-liquid crystal displays (TFT-LCD) by a fluidized bed crystallizer (FBC), RSC Adv. 7 (2017) 40819–40828, https://doi.org/10.1039/c7ra06308c.
[7] G. Simoni, B.S. Kirkebæk, C.A. Quist-Jensen, M.L. Christensen, A. Ali, A comparison of vacuum and direct contact membrane distillation for phosphorus and ammonia recovery from wastewater, J. Water Process Eng. 44 (2021), 102350, https://doi.org/10.1016/j.jwpe.2021.102350.
[8] C.A. Quist-Jensen, A. Ali, S. Mondal, F. Macedonio, E. Drioli, A study of membrane distillation and crystallization for lithium recovery from high-concentrated aqueous solutions, J. Membr. Sci. 505 (2016) 167–173, https://doi.org/10.1016/j.memsci.2016.01.033.
[9] J. Liu, X. Cheng, X. Qi, N. Li, J. Tian, B. Qiu, K. Xu, D. Qu, Recovery of phosphate from aqueous solutions via vivianite crystallization: Thermodynamics and influence of pH, Chem. Eng. J. 349 (2018) 37–46, https://doi.org/10.1016/j.cej.2018.05.064.
[10] C.A. Quist-Jensen, J.M. Sørensen, A. Svenstrup, L. Scarpa, T.S. Carlsen, H. C. Jensen, L. Wybrandt, M.L. Christensen, Membrane crystallization for phosphorus recovery and ammonia stripping from reject water from sludge dewatering process, Desalination. 440 (2018) 156–160, https://doi.org/10.1016/j.desal.2017.11.034.
[11] C.A. Quist-Jensen, M.K. Jørgensen, M.L. Christensen, Treated seawater as a magnesium source for phosphorous recovery from wastewater—A feasibility and cost analysis, Membranes (Basel). 6 (2016), https://doi.org/10.3390/membranes6040054.
[12] F. Rizzioli, D. Bertasini, D. Bolzonella, N. Frison, F. Battista, A critical review on the techno-economic feasibility of nutrients recovery from anaerobic digestate in the agricultural sector, Sep. Purif. Technol. 306 (2023), 122690, https://doi.org/10.1016/j.seppur.2022.122690.
[13] Ordinance on the reorganisation of sewage sludge recycling, Federal Law Gazette of Germany, Part I, No. 65, Vol 27, September 2017. Available online: https://www.bgbl.de/xaver/bgbl/start.xav?startbk=Bundesanzeiger_BGBl&jumpTo=bgbl117s3465.pdf#_bgbl_%2F%, 2017 (accessed 28th July 2023).
[14] R. Goedhart, S. Müller, M.C.M. van Loosdrecht, D. van Halem, Vivianite precipitation for iron recovery from anaerobic groundwater, Water Res. 217 (2022), 118345, https://doi.org/10.1016/j.watres.2022.118345.
[15] E. Frossard, J.P. Bauer, F. Lothe, Evidence of vivianite in FeSO4 - Flocculated sludges, Water Res. 31 (1997) 2449–2454, https://doi.org/10.1016/S0043-1354(97)00101-2.
[16] X. Dou, H. Huang, X. Wang, Q. Lin, J. Li, Y. Zhang, Y. Han, Collision dependent silver nucleation regulated by chemical diffusion and reaction, Chem. Eng. Sci. 262 (2022), 117965, https://doi.org/10.1016/j.ces.2022.117965.
[17] X. Dou, H. Huang, Y. Han, The role of diffusion in the nucleation of calcium carbonate, Chinese, J Chem. Eng. 43 (2022) 275–281, https://doi.org/10.1016/j.cjche.2021.03.039.
[18] R. Kieffer, D. Mangin, F. Puel, C. Charcosset, Precipitation of barium sulphate in a hollow fiber membrane contactor: Part II The influence of process parameters, Chem. Eng. Sci. 64 (2009) 1885–1891, https://doi.org/10.1016/j.ces.2009.01.013.
[19] E. Chabanon, D. Mangin, C. Charcosset, Membranes and crystallization processes: State of the art and prospects, J. Membr. Sci. 509 (2016) 57–67, https://doi.org/10.1016/j.memsci.2016.02.051.
[20] G. Di Profio, E. Curcio, E. Drioli, Supersaturation control and heterogeneous nucleation in membrane crystallizers: Facts and perspectives, Ind. Eng. Chem. Res. 49 (2010) 11878–11889, https://doi.org/10.1021/ie100418z.
[21] S. Bavarella, M. Hermassi, A. Brookes, A. Moore, P. Vale, G. Di Profio, E. Curcio, P. Hart, M. Pidou, E.J. McAdam, Is Chemically Reactive Membrane Crystallization Faciliated by Heterogeneous Primary Nucleation? Comparison with Conventional Gas-Liquid Crystallization for Ammonium Bicarbonate Precipitation in a CO2-NH3-H2O System, Cryst. Growth Des. 20 (2020) 1552–1564, https://doi.org/10.1021/acs.cgd.9b01276.
[22] E. Drioli, G. Di Profio, Curcio Efrem, Membrane-Assisted Crystallization Technology, World Scientific, London (2015), https://doi.org/10.1142/9781783263325_0001.
[23] R. Klaassen, P.H.M. Feron, A.E. Jansen, Membrane contactors in industrial applications, Chem. Eng. Res. Des. 83 (2005) 234–246, https://doi.org/10.1205/cherd.04196.
[24] J. Kuhn, R. Lakerveld, H.J.M. Kramer, J. Grievink, P.J. Jansens, Characterization and dynamic optimization of membrane-assisted crystallization of adipic acid, Ind. Eng. Chem. Res. 48 (2009) 5360–5369, https://doi.org/10.1021/ie802010z.
[25] W.T. You, Z.L. Xu, Z.Q. Dong, M. Zhang, Vacuum membrane distillation–crystallization process of high ammonium salt solutions, Desalin. Water Treat. 55 (2015) 368–380, https://doi.org/10.1080/19443994.2014.922499.
[26] J.C.W. Fern, S. Ohsaki, S. Watano, R. Pfeffer, Continuous synthesis of nano-drug particles by antisolvent crystallization using a porous hollow-fiber membrane module, Int. J. Pharm. 543 (2018) 139–150, https://doi.org/10.1016/j.ijpharm.2018.03.025.
[27] Z. Jia, Z. Liu, Synthesis of nanosized BaSO4 particles with a membrane reactor: effects of operating parameters on particles, J. Membr. Sci. 209 (2002) 153–161, https://doi.org/10.1016/S0376-7388(02)00326-5.
[28] D. Chen, B. Wang, K.K. Sirkar, Hydrodynamic modeling of porous hollow fiber anti-solvent crystallizer for continuous production of drug crystals, J. Membr. Sci. 556 (2018) 185–195, https://doi.org/10.1016/j.memsci.2018.03.046.
[29] X. Zhou, X. Zhu, B. Wang, J. Li, Q. Liu, X. Gao, K.K. Sirkar, D. Chen, Continuous production of drug nanocrystals by porous hollow fiber-based anti-solvent crystallization, J. Membr. Sci. 564 (2018) 682–690, https://doi.org/10.1016/j.memsci.2018.07.082.
[30] L. Tuo, X. Ruan, W. Xiao, X. Li, G. He, X. Jiang, A novel hollow fiber membrane-assisted antisolvent crystallization for enhanced mass transfer process control, AIChE J. 65 (2019) 734–744, https://doi.org/10.1002/aic.16438.
[31] X. Jiang, Y. Niu, S. Du, G. He, Membrane crystallization: Engineering the crystallization via microscale interfacial technology, Chem. Eng. Res. Des. 178 (2022) 454–465, https://doi.org/10.1016/j.cherd.2021.12.042.
[32] Z. Jia, Z. Liu, F. He, Synthesis of nanosized BaSO4 and CaCO3 particles with a membrane reactor: Effects of additives on particles, J. Colloid Interface Sci. 266 (2003) 322–327, https://doi.org/10.1016/S0021-9797(03)00187-5.
[33] Y. Yin, T. Li, K. Zuo, X. Liu, S. Lin, Y. Yao, T. Tong, Which Surface Is More Scaling Resistant? A Closer Look at Nucleation Theories for Heterogeneous Gypsum Nucleation in Aqueous Solutions, Environ. Sci. Technol. 56 (2022) 16315–16324, https://doi.org/10.1021/acs.est.2c06560.
[34] A. Mersmann, Crystallization and precipitation, Chem. Eng. Process. Process Intensif. 38 (1999) 345–353, https://doi.org/10.1016/S0255-2701(99)00025-2.
[35] C. Charcosset, H. Fessi, Preparation of nanoparticles with a membrane contactor, J. Membr. Sci. 266 (2005) 115–120, https://doi.org/10.1016/j.memsci.2005.05.016.
[36] R. Kieffer, D. Mangin, F. Puel, C. Charcosset, Precipitation of barium sulphate in a hollow fiber membrane contactor, Part I: Investigation of particulate fouling, Chem. Eng. Sci. 64 (2009) 1759–1767, https://doi.org/10.1016/j.ces.2009.01.011.
[37] R. Jiménez-Robles, C. Gabaldón, J.D. Badia, M. Izquierdo, V. Martínez-Soria, Recovery of dissolved methane through a flat sheet module with PDMS, PP, and PVDF membranes, Sep. Purif. Technol. 282 (2022) 1–11, https://doi.org/10.1016/j.seppur.2021.120057.
[38] M. Younas, M. Rezakazemi, in: Membrane Contactor Technology: Water Treatment, Food Processing, Gas Separation, Wiley-VCH Verlag GmbH, 2022, https://doi.org/10.1002/9783527831036.
[39] R. Jiménez-Robles, B.M. Moreno-Torralbo, J.D. Badia, V. Martínez-Soria, M. Izquierdo, Flat PVDF membrane with enhanced hydrophobicity through alkali

activation and organofluorosilanisation for dissolved methane recovery, Membranes (Basel). 12 (2022) 1–19. 10.3390/ membranes12040426.
[40] R. Jiménez-Robles, M. Izquierdo, V. Martínez-Soria, L. Martí, A. Monleón, J. D. Badia, Stability of Superhydrophobicity and Structure of PVDF Membranes Treated by Vacuum Oxygen Plasma and Organofluorosilanisation, Membranes (Basel). 13 (2023), https://doi.org/10.3390/membranes13030314.
[41] R.S. Hebbar, A.M. Isloor, A.F. Ismail, Contact Angle Measurements, in, Membrane Characterisation Book, Elsevier, 2017, pp. 219–255.
[42] L. Liu, F. Shen, X. Chen, J. Luo, Y. Su, H. Wu, Y. Wan, A novel plasma-induced surface hydrophobization strategy for membrane distillation: Etching, dipping and grafting, J. Membr. Sci. 499 (2016) 544–554, https://doi.org/10.1016/j.memsci.2015.11.003.
[43] R. Jiménez-Robles, V. Martínez-Soria, M. Izquierdo, Fouling characterisation in PVDF membrane contactors for dissolved methane recovery from anaerobic effluents: effect of surface organofluorosilanisation, Environ. Sci. Pollut. Res. 30 (2023) 29164–29179, https://doi.org/10.1007/s11356-022-24019-z.
[44] A. Mersmann, M. Kind, Chemical engineering aspects of precipitation from solution, Chem. Eng. Technol. 11 (1988) 264–276, https://doi.org/10.1002/ceat.270110136.
[45] G. Zeng, H. Li, S. Huang, X. Wang, J. Chen, Determination of Metastable Zone Width and the Primary Nucleation Kinetics of Sodium Sulfate, Theor. Found. Chem. Eng. 49 (2015) 869–876, https://doi.org/10.1134/S0040579515050309.
[46] K. Sangwal, A novel self-consistent Nývlt-like equation for metastable zone width determined by the polythermal method, Cryst. Res. Technol. 44 (2009) 231–247, https://doi.org/10.1002/crat.200800501.
[47] K.J. Kim, A. Mersmann, Estimation of metastable zone width in different nucleation processes, Chem. Eng. Sci. 56 (2001) 2315–2324, https://doi.org/10.1016/S0009-2509(00)00450-4.
[48] T. Horseman, Y. Yin, K.S. Christie, Z. Wang, T. Tong, S. Lin, Wetting, Scaling, and Fouling in Membrane Distillation: State-of-the-Art Insights on Fundamental Mechanisms and Mitigation Strategies, ACS ES&T Eng. 1 (2021) 117–140, https://doi.org/10.1021/acsestengg.0c00025.
[49] A. McLeod, P. Buzatu, O. Autin, B. Jefferson, E. McAdam, Controlling shell-side crystal nucleation in a gas-liquid membrane contactor for simultaneous ammonium bicarbonate recovery and biogas upgrading, J. Membr. Sci. 473 (2015) 146–156, https://doi.org/10.1016/j.memsci.2014.07.063.
[50] C.J. Davey, M. Hermassi, E. Allard, M. Amine, N. Sweet, T.S. Gaite, A. McLeod, E. J. McAdam, Integrating crystallisation into transmembrane chemical absorption: Process intensification for ammonia separation from anaerobic digestate, J. Membr. Sci. 611 (2020), 118236, https://doi.org/10.1016/j.memsci.2020.118236.
[51] E. Curcio, E. Fontananova, G. Di Profio, E. Drioli, Influence of the structural properties of poly(vinylidene fluoride) membranes on the heterogeneous nucleation rate of protein crystals, J. Phys. Chem. B. 110 (2006) 12438–12445, https://doi.org/10.1021/jp061531y.
[52] A. Myerson, D. Erdemir, A. Lee, Handbook of industrial crystallsiation, Third Ed., Cambridge University Press, 2019. 10.1017/9781139026949.
[53] M. Shen, Z. Lu, Y. Xu, X. He, Vivianite and Its Oxidation Products in Mammoth Ivory and Their Implications to the Burial Process, ACS Omega. 6 (2021) 22284–22291, https://doi.org/10.1021/acsomega.1c02964.